

Modeling the Dichotomy of the Immune Response to Cancer: Cytotoxic Effects and Tumor-Promoting Inflammation

Kathleen P. Wilkie^{1,2} · Philip Hahnfeldt¹

Received: 8 April 2015 / Accepted: 4 May 2017 / Published online: 5 June 2017
© Society for Mathematical Biology 2017

Abstract Although the immune response is often regarded as acting to suppress tumor growth, it is now clear that it can be both stimulatory and inhibitory. The interplay between these competing influences has complex implications for tumor development, cancer dormancy, and immunotherapies. In fact, early immunotherapy failures were partly due to a lack in understanding of the nonlinear growth dynamics these competing immune actions may cause. To study this biological phenomenon theoretically, we construct a minimally parameterized framework that incorporates all aspects of the immune response. We combine the effects of all immune cell types, general principles of self-limited logistic growth, and the physical process of inflammation into one quantitative setting. Simulations suggest that while there are pro-tumor or antitumor immunogenic responses characterized by larger or smaller final tumor volumes, respectively, each response involves an initial period where tumor growth is stimulated beyond that of growth without an immune response. The mathematical description is non-identifiable which allows an ensemble of parameter sets to capture inherent biological variability in tumor growth that can significantly alter tumor–immune dynamics and thus treatment success rates. The ability of this model to predict non-intuitive yet clinically observed patterns of immunomodulated tumor growth suggests that it may provide a means to help classify patient response dynamics to aid identification of appropriate treatments exploiting immune response to improve tumor suppression, including the potential attainment of an immune-induced dormant state.

✉ Kathleen P. Wilkie
kpwilkie@ryerson.ca

✉ Philip Hahnfeldt
Hahnfeldt@cancer-systems-biology.org

¹ Center of Cancer Systems Biology, Boston, MA, USA

² Department of Mathematics, Ryerson University, Toronto, ON, Canada

Keywords Theoretical cancer immunology · Immunoediting · Ordinary differential equations · Tumor-immune dynamics · Cancer modeling

1 Introduction

The role of the immune response in tumorigenesis is now generally accepted to be both stimulatory and inhibitory (Mantovani et al. 2008; de Visser et al. 2006). While the cytotoxic role of the immune system in tumor eradication has been known for centuries, it is only recently that the concept of immune stimulation of tumor development has become well accepted (de Visser et al. 2006; Hanahan and Weinberg 2011; Grivennikov et al. 2010; Rakoff-Nahoum 2006; Prehn 1972). One important mechanism of the pro-tumor immune response, inflammation, has been linked to tumor initiation (Kraus and Arber 2009), tumor progression (Mantovani et al. 2008; Grivennikov et al. 2010; Balkwill and Coussens 2004), and metastasis (Condeelis and Pollard 2006). Even inflammation, however, can be either stimulatory or inhibitory to tumor growth (Nelson and Ganss 2006).

The polarity of the tumor microenvironment, whether it be tumor-promoting or tumor-inhibiting, is determined by the intercellular interactions and cytokine signaling milieu. Tumor microenvironments include, among the extracellular matrix and stromal cells, a variety of innate immune cells (including macrophages, neutrophils, mast cells, myeloid derived suppressor cells, natural killer cells, and dendritic cells) and adaptive immune cells (including B and T lymphocytes). Each immune cell type may have both tumor-promoting and tumor-inhibiting actions. Macrophages, for example, can recognize and engulf cancer cells, but they can also promote tumor growth through the expression of cytokines and chemokines, which in turn stimulates angiogenesis (De Palma et al. 2005; Albini 2005), lymphangiogenesis (Ji 2012), and matrix remodeling (Condeelis and Pollard 2006). More generally, mechanisms of immune stimulation of cancer development include the induction of DNA damage by the generation of free radicals, the promotion of angiogenesis and tissue remodeling through growth factor, cytokine, chemokine, and matrix metalloproteinase production, the suppression of antitumor immune activities, and the promotion of chronic inflammation in the tumor microenvironment (de Visser et al. 2006). Mechanisms of immune inhibition of cancer development include the inhibition of tumor growth through direct cancer cell lysis, cancer cell apoptosis induced by perforin and granzymes or Fas/Fas-ligand binding, and the pro-inflammatory but antitumor production of cytokines such as IL-2, IL-12, and IFN- γ (Nelson and Ganss 2006). In fact, the shift of the inflammatory environment from pro-tumor and pro-angiogenic (with factors such as IL-4, IL-6, IL-10, and TGF- β) to antitumor and anti-angiogenic (with factors such as IL-2, IL-12, IP-10, MIG, and IFN- γ) may be crucial for tumor elimination, as even vascular endothelial cells have been shown to lyse target tumor cells once activated with TNF- α and IFN- γ (Li et al. 1991). Thus, the cytokines and growth factors present in the tumor microenvironment are not only crucial for the determination of the differentiated state of the immune response, but also for the determination of the response of local stromal cells to tumor presence.

Tumor microenvironments can be modified by the adaptive immune response, and this effect can be enhanced by immunotherapy (Nelson and Ganss 2006). Cancer immunotherapy aims to improve tumor suppression by increasing cytotoxic strength. One type of cytokine immunotherapy involves the repeated injection of IL-2, which primes the T cell response with CD4⁺ and CD8⁺ T cells. With intratumoral injection of IL-2, tumor regression was shown to correlate with a reduction in tumor blood vessels and this process was shown to be dependent on functional CD8⁺ lymphocytes (Jackaman et al. 2003). The efficacy of this treatment, however, declined with increasing tumor size, which may be associated with a less effective immune response. The ability of the immune response to modify tumor vasculature suggests a potential anti-cancer strategy of cytokine-based immunotherapy, with inflammatory factors such as IFN- γ , to shift the pro-angiogenic and immunosuppressive tumor microenvironment to an anti-angiogenic microenvironment that supports cytotoxic immune activities. These cytotoxic activities could then be enhanced by cell-based immunotherapies such as adoptive T cell transfer or dendritic cell activation (Nelson and Ganss 2006). Figure 1 summarizes the significant immune cells and cytokines or growth factors involved in the pro-tumor and antitumor inflammatory responses.

To identify and track the complex mechanistic interplays underlying tumor development in the context of the immune response, we sought to distill the fundamental reciprocal interactions controlling the process into one quantitative framework. Heretofore, several approaches have been applied to quantify cancer-immune interactions. Perhaps the most common is to describe the system as a set of ordinary differential equations that capture the time-varying dynamics at the population level (DeLisi and Rescigno 1977; Kuznetsov et al. 1994; Kirschner and Panetta 1998; de Pillis et al. 2005; d'Onofrio 2005; d'Onofrio and Ciancio 2011; Eftimie et al. 2010; Wilkie 2013; Wilkie and Hahnfeldt 2013). Other approaches focus on random effects with stochastic differential equations (Lefever and Horsthemke 1978), spatio-temporal dependence with partial differential equations (Matzavinos et al. 2004; Roose et al. 2007; Al-Tameemi et al. 2012), and individual cell-cell interactions using agent-based methods (Takayanagi et al. 2006; Roose et al. 2007; Enderling et al. 2012). Among the several excellent reviews on the subject are those covering discrete tumor-immune competition approaches (Adam and Bellomo 1997), non-spatial, time-varying models (Eftimie et al. 2010), and analyses of the dormant or near-dormant tumor state (Wilkie 2013).

Despite the overwhelming evidence of direct immune stimulation of tumor growth, mathematical treatments of tumor-immune interactions have, until recently, focused solely on the cytotoxic actions of immune cells. Two new models describe immune stimulation of tumor growth directly, through an increased basal growth rate (den Breems and Eftimie 2016; Louzoun et al. 2014). Others describe it indirectly as a by-product of cytotoxic inhibitory actions (Kuznetsov 1988; Joshi et al. 2009). We show here that inclusion of immune stimulation, through increased tumor growth rate and carrying capacity, explain observations of tumor promotion prior to tumor suppression over the course of immunotherapy (Wolchok et al. 2009). Importantly, observations of this early tumor promotion contributed to the failure of many early immunotherapy programs (Hoos 2012). The model presented here demonstrates that such unexpected outcomes are in fact a natural consequence of the dichotomous roles of the immune

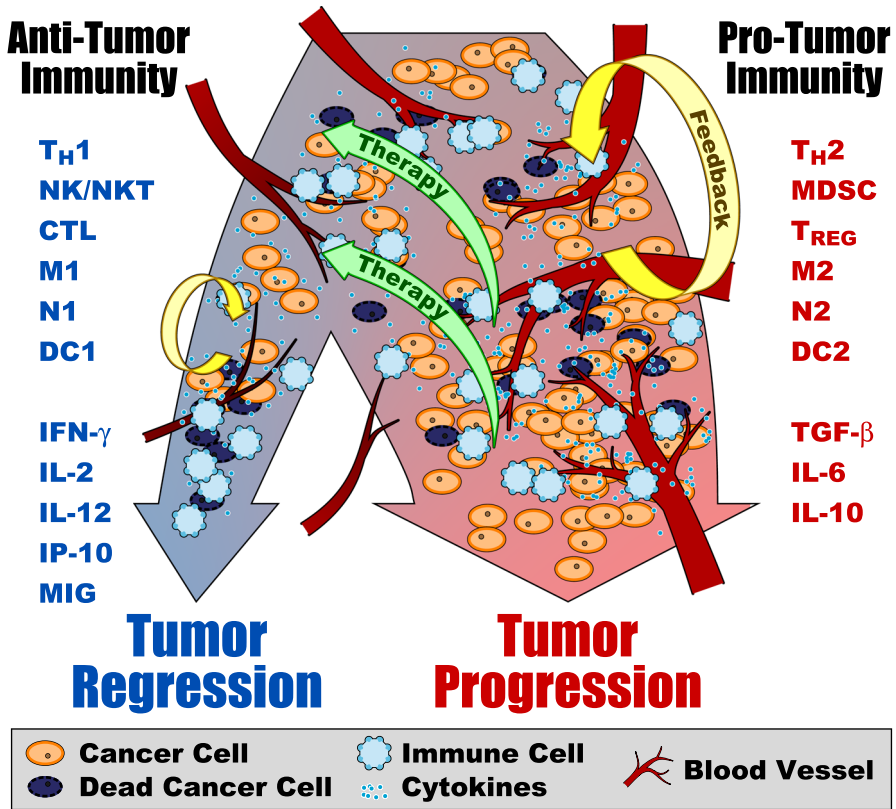


Fig. 1 Pro-tumor and antitumor inflammatory responses are composed of different (or differently polarized) immune cells and cytokines/growth factors. The cytokine milieu present in the environment determines the polarization of newly differentiating immune cells. The cytokines produced by these new cells allows for a strong feedback mechanism to enhance the polarity of the immune response. Over time, these mechanisms may lead to the development of either a pro-tumor immunity that enhances vascularization and tumor progression, or an antitumor immunity that reduces vascularization and enhances tumor regression. Therapies that target the immune cells and cytokines present in the environment attempt to shift a pro-tumor immunity to an antitumor immunity to improve tumor suppression (Color figure online)

response. Below, we present and analyze a mathematical framework that incorporates both immune-mediated tumor stimulation and inhibition. This new model is capable of analyzing a more complete view of the interactions between cancer and immune cells, and is therefore more suited for analysis and prediction of cancer treatment strategies, especially immunotherapies.

2 Model Equations and Assumptions

In this work, cancer and immune cell populations are assumed to grow according to a generalized logistic law that is mechanistically modified by their cellular interactions. A brief review of a generalization of this model can be found in [Kareva et al. \(2014\)](#).

2.1 Cancer Population Growth

The cancer population, $C(t)$, grows intrinsically up to a limiting size, the carrying capacity $K_C(t)$, according to generalized logistic growth. Recall that generalized logistic growth has the form:

$$\frac{dC}{dt} = \frac{\mu}{\alpha} C \left(1 - \left(\frac{C}{K_C} \right)^\alpha \right)$$

where $\frac{\mu}{\alpha}$ is the unregulated growth rate, μ is the “intrinsic” growth rate, and α is the reciprocal of the strength of regulation that the carrying capacity imposes on the population. Notice that $\alpha = 1$ gives regular logistic growth, and the limit as $\alpha \rightarrow 0$ (or $\frac{1}{\alpha} \rightarrow \infty$, very strong regulation), gives Gompertzian growth ($\frac{dC}{dt} = \mu C \ln \left(\frac{K_C}{C} \right)$), both with growth rate μ .

In this model, cancer growth is inhibited by the immune system through predation, $\Psi = \Psi(I, C) \leq 0$, which modulates the growth rate (discussed later), and it is stimulated by the immune system through an inflammatory process incorporated in the carrying capacity, $K_C = K_C(I, C)$. The cancer population is thus governed by

$$\frac{dC}{dt} = \frac{\mu}{\alpha} (1 + \Psi) C \left(1 - \left(\frac{C}{K_C} \right)^\alpha \right), \quad C(0) = C_0. \tag{1}$$

The carrying capacity is determined by a balance of stimulatory (pro-angiogenic) and inhibitory (anti-angiogenic) terms. Based on a diffusion-consumption partial differential equation and arguments of the relative clearance rates for pro- and anti-angiogenic signals, it was suggested (Hahnfeldt et al. 1999) that the stimulation term be proportional to tumor volume to the power 1 (say V^1) and that the inhibition term be proportional to tumor volume to the power $\frac{5}{3}$, (or $V^{\frac{5}{3}}$). We modify these terms to include the pro- and anti-angiogenic signals produced by immune cells also present in the tumor mass, in addition to those produced by cancer cells. Hence, we assume that pro-angiogenic signals produced by cancer cells, immune cells, and their interactions, are proportional to volume to the first power: that is, $V^1 \propto (B + I)^a C^{1-a}$, where B is a background constant enabling the cancer to stimulate its own growth in the absence of an immune response and a is the weight of immune contribution, $0 \leq a \leq 1$.

Similarly, cancer cells, immune cells, the current microenvironment, and their interactions, produce anti-angiogenic signals in proportion to volume to the $5/3$ rd power: that is $V^{\frac{5}{3}} \propto K_C^1 (B + I)^b C^{\frac{2}{3}-b}$, where b is the weight of immune contribution, $0 \leq b \leq \frac{2}{3}$. The choice of weights K_C^1 and $C^{\frac{2}{3}}$ were suggested in Hahnfeldt et al. (1999). Taken together, this mathematical formulation allows both pro- and anti-angiogenic signals to be produced by cancer cells, immune cells, and their interactions. Defining $B = 1$ allows for cancer growth without any extrinsic stimulation, and thus the cancer carrying capacity is governed by

$$\frac{dK_C}{dt} = p(1 + I)^a C^{1-a} - qK_C(1 + I)^b C^{\frac{2}{3}-b}, \quad K_C(0) = K_{C,0}, \tag{2}$$

where p is the stimulation coefficient and q is the inhibition coefficient.

We assume that the majority of these signals should originate from the cancer population and thus require a and b to be small. Again, a controls the weight of immune-produced tumor-promoting factors (i.e. pro-angiogenic signals) that act to increase the tumor’s carrying capacity, and b controls the weight of immune-produced tumor-inhibiting factors (i.e. anti-angiogenic signals) that act to limit the tumor’s carrying capacity. A pro-angiogenic tumor-promoting inflammatory microenvironment is associated with immunosuppressive myeloid cells, Th2 immunity, and cytokines such as TGF- β , IL-4, IL-6, and IL-10 (DeNardo et al. 2010). Cytotoxic T cell activity, Th1 immunity, and cytokines such as IFN- γ , IL-2, and IL-12 are significant factors contributing to an anti-angiogenic tumor-inhibiting inflammatory microenvironment (Nelson and Ganss 2006). See Fig. 1.

When $a > b$, more weight is placed on immune-mediated tumor-promoting effects than tumor-inhibiting effects, and we label this case as *pro-tumor immunity*. When $a < b$, more weight is placed on immune-mediated tumor-inhibiting effects and we label this case as *antitumor immunity*. In this work, we chose $a = \frac{2}{10}$, which allows immune cells to contribute to tumor promotion but requires the majority of stimulation to originate from the tumor itself. We then choose $b = \frac{1}{10}$ (a value slightly less than a) for pro-tumor immunity and $b = \frac{3}{10}$ (a value slightly greater than a) for antitumor immunity.

2.2 Immune Population Growth

The immune population, $I(t)$, which includes all various immune cell types, is governed by logistic growth and maintains a homeostatic (equilibrium) healthy level, I_e . In the healthy state when $C = 0$ the carrying capacity is this homeostatic level: $K_I = I_e$. Immune population growth is stimulated by the cancer’s presence through direct recruitment, rC , and through cancer-immune interactions that increase the carrying capacity, $K_I = K_I(I, C)$, giving:

$$\frac{dI}{dt} = \lambda (I + rC) \left(1 - \frac{I}{K_I} \right), \quad I(0) = I_0, \tag{3}$$

where λ is the unregulated growth rate and r is the cancer-induced recruitment parameter. Note that logistic growth is assumed here for simplicity and a lack of experimental data on immune growth dynamics.

The associated carrying capacity is determined by a balance of stimulatory, inhibitory, and homeostatic terms:

$$\frac{dK_I}{dt} = xI^{\frac{1}{2}}C^{\frac{1}{2}} - yK_I I^{\frac{1}{3}}C^{\frac{1}{3}} - z(K_I - I_e), \quad K_I(0) = K_{I,0}. \tag{4}$$

where x , y , and z , are the stimulation, inhibition, and homeostatic coefficients, respectively. Following the same arguments as used in determining the cancer carrying capacity, the stimulation term above prescribes equal weight to the two popula-

tions, giving $V^1 \propto I^{\frac{1}{2}}C^{\frac{1}{2}}$. And the inhibition term, prescribing equal weight, is $V^{\frac{5}{3}} \propto K_I I^{\frac{1}{3}}C^{\frac{1}{3}}$. Control of the immune response is obtained through the actions of checkpoint blockades and regulatory T cells, as well as other mechanisms, and thus is determined by cancer-immune interactions. The last term on the right-hand side represents an organismic tendency of the immune response to return to a healthy homeostatic state after disease elimination.

2.3 Immune Predation of Cancer Cells

The dynamics of cytotoxic immune actions targeted against cancer cells depend on the specific immune cell types. Here, we include all types, and model predation by

$$\Psi = -\theta \left(\frac{I^\beta}{\phi C^\beta + I^\beta} + \epsilon \log_{10}(1 + I) \right), \quad (5)$$

where the term $\frac{\theta I^\beta}{\phi C^\beta + I^\beta}$ describes the saturation kinetics of strong cytotoxic actions (de Pillis et al. 2005) and the term $\epsilon \theta \log_{10}(1 + I)$ allows for a gradual increase to this saturation level with significant increase in immune presence. Here, θ is the saturation maximum, and ϕ and β are saturation shape parameters. The ratio-dependent saturation term was shown to describe cytotoxic effects of T cells (de Pillis et al. 2005), but we also require contributions from innate immunity (natural killer cells and macrophages) which does not exhibit saturation in cytotoxic assays (Diefenbach et al. 2001). The logarithmic term accounts for innate immunity at large population sizes and phenomenologically maps the actions into a range appropriate for Ψ . For small immune populations, innate and adaptive predation can be combined into the ratio-dependent term, but for large populations, innate immunity should still have some effect (here we assume it small and set $\epsilon = 0.01$). Without an increasing predation threshold, tumor growth dynamics, especially after periods of immune-induced tumor dormancy, would not reflect the still growing immune presence, which could have significant implications on immunotherapy predictions. Thus, this form accounts for adaptive and innate cytotoxic effects over a wide range of immune population sizes, which are both required for tumor elimination (Koebel et al. 2007).

Note that in Eq. (1), immune predation is a multiplicative factor. This implies that when the cancer population reaches capacity and cancer growth stops, effective immune predation is also restricted. That is, once capacity is reached, the immune response cannot change this fate. This form models the biological resistance mechanisms cancer cells develop to overcome immune attack: namely physical overcrowding leading to difficult immune penetration into the mass and immune checkpoint activation through CTLA-4 and PD1, for example Pardoll (2012).

3 Experimental Data and Parameter Estimation

Equations (1)–(4) govern a system of four dependent variables, $C(t)$, $I(t)$, $K_C(t)$, and $K_I(t)$, which describe the growth dynamics of a tumor in the presence of a com-

plete and competent immune system capable of both stimulating and inhibiting cancer growth. Parameters for tumor growth are estimated in stages using a Markov Chain Monte Carlo (MCMC) method (Robert and Casella 2010; Cirit and Haugh 2012). From an initial guess, a Markov chain of permitted parameter sets is created by randomly perturbing the previous parameter set and accepting this perturbed set with a probability determined by a measure of the goodness of fit, here the sum of squared deviations. Each parameter is perturbed and tested for acceptance independently, except parameters μ and α , which are perturbed and tested together since they are inherently related in Eq. (1) as the unregulated growth rate $\frac{\mu}{\alpha}$.

Tumor growth parameters ($\mu, \alpha, p, q, K_{C,0}$) and the immune homeostatic parameter (I_e) are estimated from subcutaneous fibrosarcoma growth data (Tanooka et al. 1982). These tumors, grown in wild-type (immune competent) mice, are nonimmunogenic due to early immunoediting (Cohen et al. 2010) and contain regulatory T cells which inhibit immune-mediated tumor rejection (Betts et al. 2007). We therefore assume that growth after the tumor reaches the palpable size of about 1.3×10^7 cells occurs in a host with negligible immune recruitment or immune predation. This simplifying assumption sets $\frac{dI}{dt} = \frac{dK_I}{dt} = 0$ in Eqs. (3) and (4), maintaining immune presence at the homeostatic level $I(t) = K_I(t) = I_e$, and it sets $\Psi = 0$ in Eq. (1), enforcing zero immune predation. This assumption underestimates the role of immune stimulation in tumor growth, but we accept this limitation in favor of simplifying the parameterization procedure.

To estimate the tumor growth parameters, our MCMC method was run 10 times with 20,000 trials per parameter in each run. Fitting Eqs. (1) and (2) with $a = \frac{2}{10}$, $b = \frac{3}{10}$, $C_0 = 1.3 \times 10^7$, and $I(t) = K_I(t) = I_e$, to the experimental growth data gives the 10 parameter sets for antitumor immunity listed at the top of Table 1. Fitting the same equations to the data with $b = \frac{1}{10}$ gives the 10 parameter sets for pro-tumor immunity listed at the bottom of Table 1. See “Appendix 1” for antitumor and pro-tumor predicted growth curves fitted to data.

This approach results in two ensembles of 10 parameter sets, one for antitumor immunity and one for pro-tumor immunity. Due to limited experimental data and the necessary level of complexity in our mathematical model, some parameter values are non-identifiable, as seen through the variability of the 10 sets, see Table 1 and “Appendix 2”. The problem of parameter identifiability is becoming increasingly important, especially in the growing areas of nonlinear ODE modeling with applications to biological networks and immune models for viral infections and cancer. It may be resolved by measuring or acquiring additional data (which may not be possible) or by model reduction, techniques of which are still under development (Miao et al. 2011; Meshkat et al. 2011; Raue et al. 2011). Our approach is to instead generate an ensemble of parameter sets that represent 10 individual in-silico patients with their own inherent variabilities instead of considering one parameter set representing an “average responder” (or one local minima in a very complex parameter space). This ensemble approach allows one to better explore the implications of cancer-immune interactions on tumor growth dynamics for a population of individuals.

To estimate immune predation parameters, we use experimental data for tumor growth resulting from co-injections of specifically trained immune cells and fibrosar-

Table 1 Antitumor and pro-tumor immunity parameter sets resulting from 10 runs of the MCMC parameter estimation method (at 20,000 iterations) which fit Eqs. (1) and (2) with $b = \frac{3}{10}$ (antitumor) or $b = \frac{1}{10}$ (pro-tumor) and $I(t) = I_e$, a constant, to the tumor growth data from Tanooka et al. (1982) using the initial guess of $(\mu, \alpha, p, q, K_{C,0}, I_e) = (1, 1, 1, 10^{-6}, 3C_0, 10^5)$

Parameter set	Minimum SSD	"Intrinsic" growth rate μ (day ⁻¹)	Growth rate regulation by carrying capacity α (1)	Cancer carrying capacity stimulation coefficient p (day ⁻¹)	Cancer carrying capacity inhibition coefficient q [(cell no.) ^{-2/3} day ⁻¹]	Initial cancer carrying capacity $K_{C,0}$ (cell no.)	Homeostatic immune population level I_e (cell no.)
<i>Antitumor immunity</i>							
1	3.66	0.29	1.31	111.38	7.85×10^{-5}	4.51×10^6	28,50
2	3.89	0.34	1.46	20.07	9.54×10^{-6}	9.11×10^6	1294
3	4.00	0.29	1.23	18.39	8.52×10^{-6}	4.54×10^6	7612
4	7.20	8.81	42.63	4.61	1.86×10^{-6}	3.02×10^7	1850
5	4.81	0.88	4.09	5.79	2.42×10^{-6}	2.88×10^7	3363
6	3.53	0.43	1.94	10.81	4.72×10^{-6}	4.55×10^7	3635
7	3.76	0.53	2.44	7.39	3.02×10^{-6}	4.09×10^7	4964
8	3.75	0.59	2.73	7.53	3.19×10^{-6}	5.11×10^7	3993
9*	12.78	0.17	1.26×10^{-7}	47.49	3.42×10^{-5}	1.72×10^4	0.41
10	5.43	1.29	6.16	5.07	2.04×10^{-6}	7.43×10^7	3156
<i>Pro-tumor immunity</i>							
1	3.21	0.33	1.34	8.52	1.43×10^{-7}	2.81×10^7	2669
2	3.22	0.44	1.91	8.95	1.38×10^{-7}	3.24×10^7	985
3*	5.67	0.23	0.43	9.24	1.37×10^{-7}	4.50×10^6	1237
4	3.48	0.55	2.55	9.43	1.28×10^{-7}	8.91×10^7	374
5	4.49	0.21	0.77	35.74	4.17×10^{-7}	3.76×10^5	93
6	3.10	0.34	1.39	8.70	1.46×10^{-7}	4.27×10^7	2914

Table 1 continued

Parameter set	Minimum SSD	"Intrinsic" growth rate μ (day ⁻¹)	Growth rate regulation by carrying capacity α (1)	Cancer carrying capacity stimulation coefficient p (day ⁻¹)	Cancer carrying capacity inhibition coefficient q [(cell no.) ^{-2/3} day ⁻¹]	Initial cancer carrying capacity $K_{C,0}$ (cell no.)	Homeostatic immune population level I_e (cell no.)
7	3.34	0.37	1.46	9.66	1.50×10^{-7}	2.55×10^7	667
8	2.86	0.37	1.70	13.55	1.91×10^{-7}	2.46×10^8	466
9	3.26	0.29	1.22	11.72	2.00×10^{-7}	3.17×10^7	2483
10	3.04	0.33	1.39	11.28	1.71×10^{-7}	5.55×10^7	863

The goodness of fit is measured by the sum of squared deviations (SSD) and the parameter set giving the minimum SSD is listed. Each parameter set fits the data equally well (see "Appendix 1"). Most parameter sets predict regions of tumor escape and elimination (see phase portraits in "Appendix 3"). Those that predict little-to-no region of tumor elimination are denoted as outlier parameter sets and are indicated here by *. Note that the data fitting assumes $C_0 = 1.3 \times 10^7$, if C_0 is changed for a simulation, the original ratio of $1.3 \times 10^7 / K_{C,0}$ is maintained by appropriately scaling $K_{C,0}$.

Table 2 Parameter values for pro- or antitumor immunity, and immune predation, growth, and recruitment

Antitumor immunity (chosen such that $a < b$, both small)	$a = \frac{2}{10}$ Weight of tumor-promoting immune function	$b = \frac{3}{10}$ Weight of tumor-inhibiting immune function	
Pro-tumor immunity (chosen such that $a > b$, both small)	$a = \frac{2}{10}$ Weight of tumor-promoting immune function	$b = \frac{1}{10}$ Weight of tumor-inhibiting immune function	
Immune predation (estimated from data in Prehn 1972)	$\theta = 2.5$ Saturation kinetic maximum	$\phi = 50$ Saturation shape parameter	$\beta = 0.5$ Saturation shape parameter
Immune growth/recruitment	$\lambda = 0.2$ (day ⁻¹) Unregulated growth rate	$r = 0.001$ Recruitment rate	
Immune carrying capacity regulation	$x = 6$ (day ⁻¹) Stimulation coefficient	$y = 10^{-7}[(\text{cell no.})^{-2/3}$ day ⁻¹] Inhibition coefficient	$z = 0.09$ (day ⁻¹) Homeostatic coefficient

The homeostatic immune presence parameter, I_e , is determined by the MCMC fitting method and is thus specific to each parameter set listed in Table 1

coma cells (Prehn 1972). In these experiments, mice were subjected to whole body irradiation and thymectomized so that host immunity is negligible. Thus, the injected immune cells are the only immune cells present in the system; their actions may be stimulatory or inhibitory to tumor growth, but it is assumed that no immune recruitment or proliferation may occur. Again, this allows us to simplify the equations by setting $\frac{dI}{dt} = \frac{dK_I}{dt} = 0$ in Eqs. (3) and (4).

In Prehn's experiment, varying numbers of splenocytes were mixed with 10^4 sarcoma cells, injected subcutaneously, and allowed to grow until the largest tumor reached a diameter of 10 mm. Results suggest that specifically trained immune cells stimulate tumor growth when mixed at ratios smaller than parity and inhibit tumor growth when mixed at ratios larger than parity. This dose-response curve was idealized to a parabolic shape with a maximum located at cancer-immune parity (Prehn 2007, 1972).

To estimate immune predation parameters θ , ϕ , and β from Eq. (5), these parameters were manually tuned (via trial and error over a broad range of values) until maximal tumor stimulation occurred near cancer-immune parity and tumor elimination occurred with sufficient immune presence, recapitulating the parabolic shape. The resulting parameter estimates are listed in Table 2.

The final stage of parameterization involves estimating parameters that describe immune growth and recruitment in the wound healing process. Due to a lack of experimental data, we estimate these parameters based on the assumption that the immune response should grow approximately as fast and as large as the tumor mass. These parameter values are also listed in Table 2.

4 Numerical Simulations and Results

Ten parameter sets are estimated using an MCMC method for both the antitumor and pro-tumor immunity cases, see Table 1. Significant variability exists in the numerical values for each parameter and yet each set fits the experimental data equally well (see Table 1 and “Appendices 1 and 2”). This parameter variability can cause significant changes in the phase-space (cancer–immune dynamics) of the model, as shown by the phase portraits in “Appendix 3”. Figure 2a shows the phase-space dynamics for an average and an outlier parameter set from both the antitumor and pro-tumor immunity cases. Outlier parameter sets were identified visually from “Appendix 3” by choosing

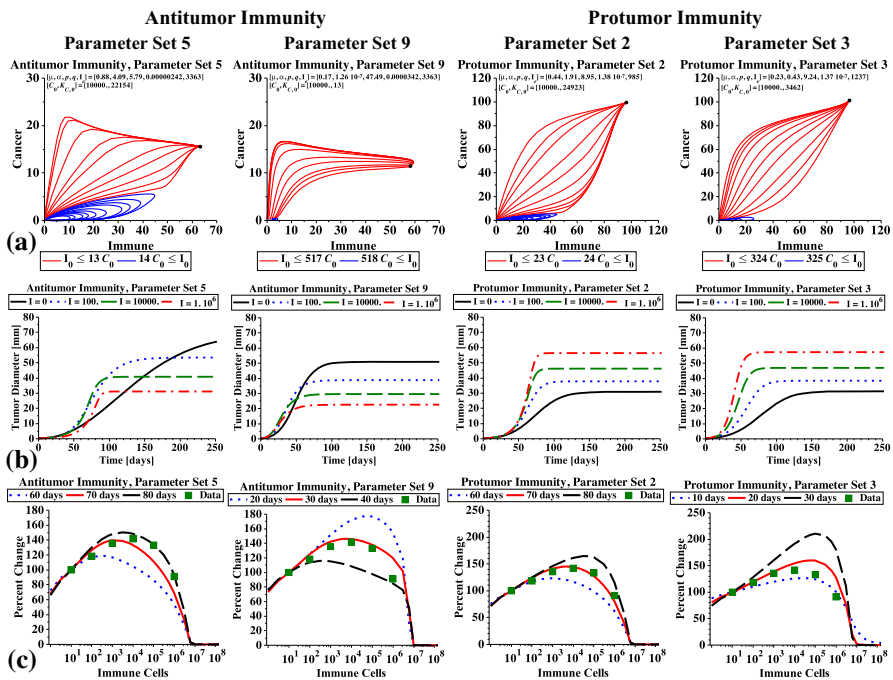


Fig. 2 The behavior of antitumor and pro-tumor immunity with both typical (sets 5 and 2) and outlier (sets 9 and 3) parameter sets. Phase portraits (a) demonstrate cancer–immune dynamics. The effect of parameter variability is demonstrated by the striking differences apparent between these phase portraits. Tumors are simulated to grow from an initial injection of $C_0 = 10^4$ cancer cells and varying numbers of immune cells ($I_0 = \gamma C_0$). The ranges (values of γ) that divide the behavior between tumor growth (red) or tumor suppression (blue), are listed below the plots. Simulations result from solving the full system of equations (1)–(4) with direct predation through Ψ , Eq. (5). Axes indicate diameter of spherical population in mm. Immune stimulation with (c) and without (b) predation is demonstrated. In (b) tumors are simulated to grow from an initial injection of 10^4 cancer cells mixed with 0 (solid black), 100 (dotted blue), 10^4 (dashed green), or 10^6 (dash-dotted red) immune cells. Simulations result from solving Eqs. (1) and (2) with $I(t)$ and $K_I(t)$ constant and $\Psi = 0$. In (c), tumors are simulated to grow from an initial injection of 10^4 cancer cells mixed with varying numbers of immune cells ranging from 0 to 10^8 . Three time snapshots of the dose–response (in terms of percent change after the indicated number of days) are shown in each plot along with the experimental data (Prehn 1972). Simulations result from solving Eqs. (1) and (2) with $I(t)$ and $K_I(t)$ constant and Ψ given by Eq. (5) (Color figure online)

the phase portraits that predicted little-to-no elimination range (set 9 for antitumor and set 3 for pro-tumor immunity).

The functional form of Eq. (2), describing the cancer carrying capacity, incorporates effects of both immune-mediated stimulation and inhibition. Figure 2b shows the effect of constant immune presence on tumor growth in both antitumor ($a < b$) and pro-tumor ($a > b$) environments without predation ($\Psi = 0$). Under this assumption, antitumor immunity stimulates tumor growth but also limits the final tumor burden. That is, the tumor may initially grow faster with immune stimulation, but the maximum obtainable size is ultimately reduced. In fact, the amount of this early-stimulation and late-inhibition arising from immune presence is sensitive to the tumor growth parameters, and thus is a feature inherent to the individual tumor, the tumor's microenvironment, and the host. When pro-tumor immunity is assumed, however, more weight is placed on the pro-angiogenic activities of inflammation and, as a result, tumors are predicted to grow faster and larger than those predicted to grow without immune presence.

The pro-tumor and antitumor cases present two fundamentally different classes of possible outcomes: immunomodulation causing tumors to grow faster but be ultimately smaller, or faster and ultimately larger, than those growing in the absence of an immune response. When $a = b$ in Eq. (2), immune stimulation of tumor growth is predicted, causing the tumors to grow faster in the presence of immune cells, but the ultimate tumor size is fixed and independent of immune presence.

Dose–response curves for both pro-tumor and antitumor immunity are shown in Fig. 2c. Again, average and outlier parameter sets are shown for each type of immunity. Tumors are simulated to grow with varying initial numbers of immune cells, predation is included but no immune growth occurs. Dose–responses at three time points are compared to the experimental data from Prehn (1972). Average and outlier parameter sets behave differently (hence the different time points used and indicated in each figure plot), but all predict immune-mediated stimulation and inhibition of tumor growth according to a parabolic shape. Importantly, the model is able to predict the ratio-dependence of tumor stimulation by immune cells, as observed by Prehn. That is, immune stimulation of tumor growth occurs when cancer cells outnumber immune cells and inhibition occurs when immune cells outnumber cancer cells.

As the phase portraits in Fig. 2a demonstrate, ultimate tumor fate is determined by the initial conditions of this deterministic model. Biologically, this may translate to the level and polarization of the immune response once the cancer reaches a critical size. Biological determinants of immune presence when the critical cancer size is reached may include the antigenicity of the cancer cells, which is related to their accumulated mutations, and the location of the cancer, as different tissues have different levels of immune surveillance. To compare our simulations, we say that this critical size is the same as our initial cancer size, $C_0 = 10^4$ cells, and thus relate the initial immune presence to this value via $I_0 = \gamma C_0$, where γ is a constant. The integer bounds for γ for each parameter set (found numerically) are shown in the figures of “Appendix 3”. Each parameter set has a different threshold value for γ , wherein immune presence less than γC_0 results in tumor escape and that greater than γC_0 in elimination. Before these dichotomous outcomes are achieved, however, seemingly contradictory events may occur, such as a transient period of dormancy prior to tumor escape, or growth and stimulation prior to elimination.

Pro-tumor inflammatory environments likely have immunosuppressive mechanisms that reduce predation efficacy. Such mechanisms, not yet considered by this model, may alter the predation parameters ϕ , β , and θ , and thus the dose–response curves predicted here. Furthermore, this framework does not allow for the evolution of antitumor immunity into pro-tumor immunity during tumor development. We note that excluding these immunosuppressive and immunoevasive mechanisms are limitations of our model and leave them to future work.

For improved tumor control, the polarization of the microenvironment should be shifted from pro-tumor to antitumor immunity via immunotherapies. We thus focus on antitumor immunity for parameter sensitivity using a parameter set demonstrating typical behavior (set 5 from Table 1). Immunotherapies that enhance the antigenicity of cancer cells can be incorporated into the model through the immune recruitment parameter r . Increases in recruitment result in improved tumor suppression and a reduction in tumor stimulation, as shown in Fig. 3.

Effects of variations in homeostatic regulation, z , are also shown in Fig. 3. As resistance to altering the immune homeostatic state is increased, tumor suppression is reduced and immune-mediated dormancy may become more difficult to achieve. As seen in Fig. 3c, increased homeostatic resistance slows immune growth, requiring higher initial immune presence for elimination. Thus, with increased homeostatic resistance, dormant tumors appear smaller and require larger initial immune presence to be obtained. Biologically, this may translate into periods of tumor dormancy for only highly immunogenic cancers in hosts with large homeostatic resistances, a parameter that may change with host health and age. Homeostatic regulation is an intrinsic patient-specific parameter that is often neglected in mathematical models, however, as demonstrated here, it may significantly affect tumor growth dynamics, and in particular, tumor dormancy. Increased immune recruitment, on the other hand, seems to improve tumor suppression while maintaining the ability to achieve a dormant tumor state, Fig. 3d.

Contour plots for parameter sensitivity are shown in Fig. 4 for the following immune-related parameter pairs: homeostasis and recruitment (r , z), immune growth rate and predation efficacy (λ , θ), and predation shape parameters (β , ϕ). For each pair three time points are shown. After 150 days, most of the predicted tumor fates have already been established. That is, either the tumor has been eliminated or escaped. Of interest, are the intermediate regions as they represent tumors whose fates may be altered through immunotherapies to achieve elimination or prolong dormancy. Since immune-induced dormancy is observed in experimental models (Quesnel 2008), parameters predicted to modify this state, such as homeostatic strength or immune recruitment, may be desirable targets for immunotherapy. In Fig. 4, the intermediate shades are intervention windows, or parameter ranges where intervention can affect tumor fate. The paired plots suggest alternate intervention strategies. For example, to achieve elimination in Fig. 4b, one can aim to increase λ , increase θ , or both, if possible. Since these windows shrink considerably over time, combination therapies may be necessary to re-open the window for immune intervention.

Figure 5 demonstrates parameter sensitivity for immune-related model parameters on atypical tumor growth behavior (outlier antitumor parameter set 9 from Table 1). With this parameter set, the model does not predict significant dormant periods prior

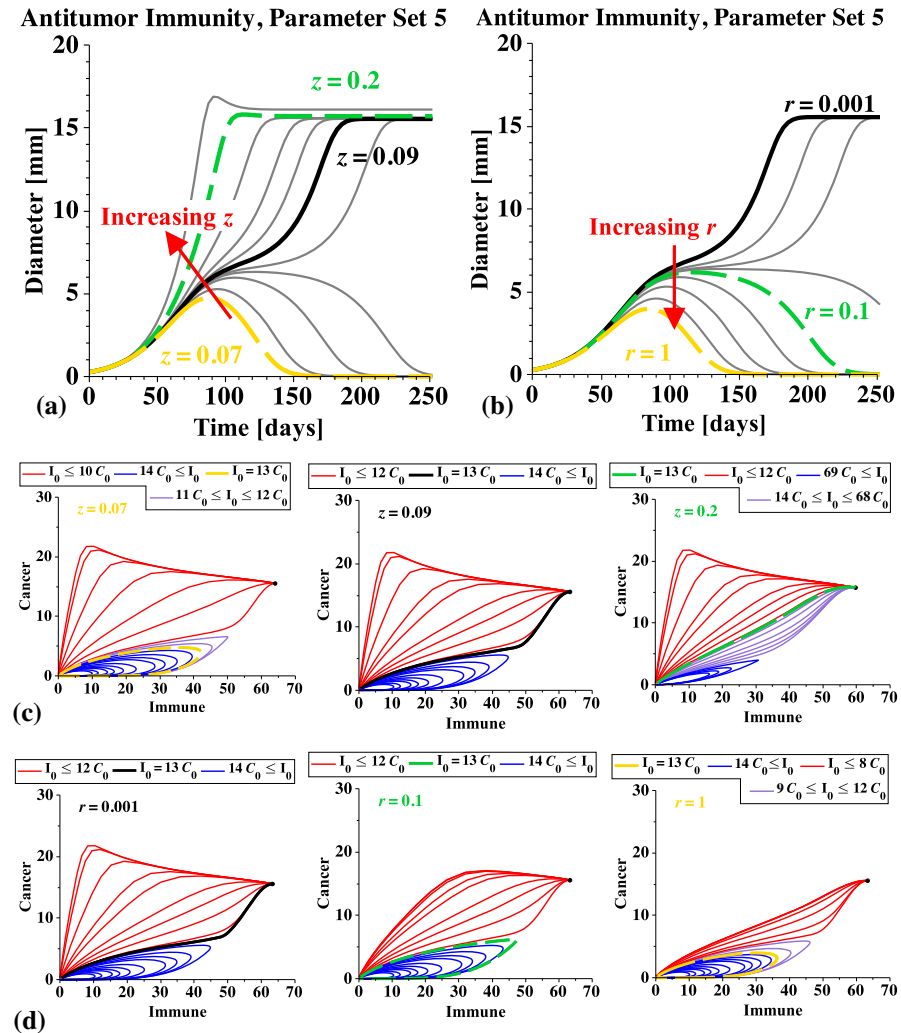


Fig. 3 Parameter sensitivity for the homeostasis parameter z (a) and the immune recruitment parameter r (b) with the corresponding phase portraits (c, d) for antitumor immunity ($a < b$) and parameter set 5 from Table 1. Phase portraits are shown in (c) for three different values of the immune homeostasis parameter z corresponding to the highlighted curves in (a). Increasing immune homeostatic resistance results in reduced tumor suppression and possibly a decreased ability to achieve tumor dormancy. Phase portraits are shown in (d) for three different values of the immune recruitment parameter r corresponding to the highlighted curves in (b). Increasing immune recruitment results in a reduction of tumor stimulation and improved tumor suppression (Color figure online)

to elimination. For immune recruitment and homeostasis parameters, larger changes are required to see an alteration in tumor fate compared to set 5. An increased immune growth rate of $\lambda = 0.4$, for example, may delay tumor growth, but not alter the fate (compare contour plots at 50 and 100 days). Comparing Figs. 3 and 4 to Fig. 5 demonstrates that treatment outcomes depend on the intrinsic growth dynamics that are captured here by the parameter ensembles of Table 1. For example, a treatment

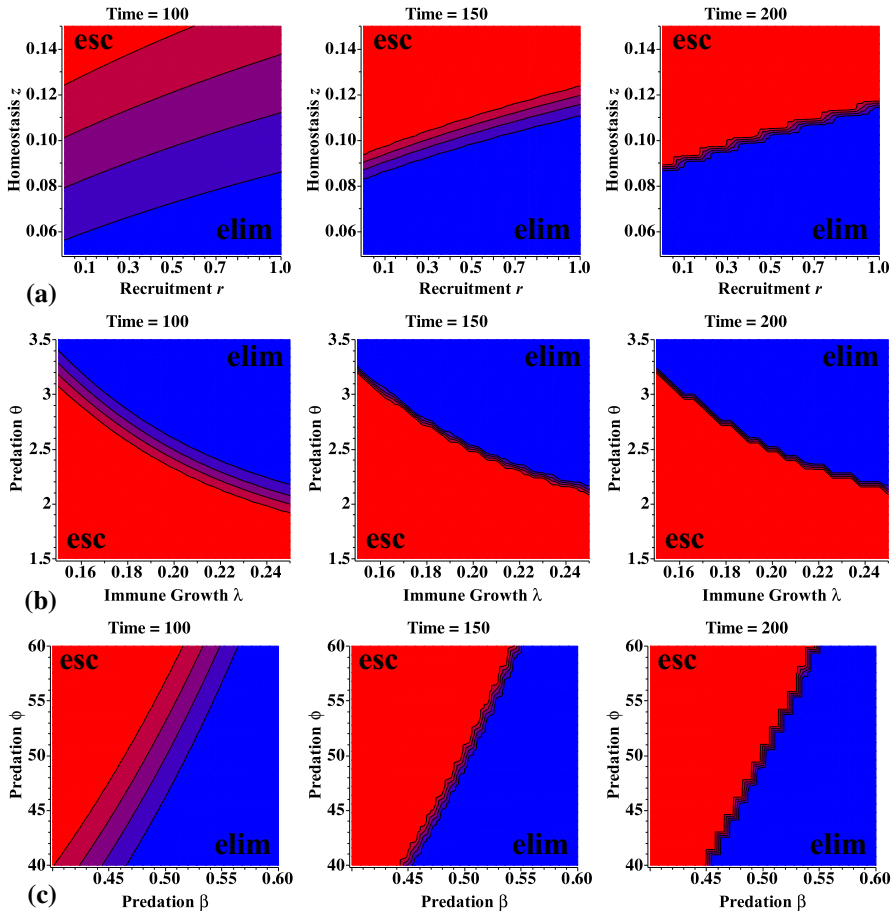


Fig. 4 Parameter sensitivity contour plots of tumor fate for the parameter pairs (r, z) , (λ, θ) , and (β, ϕ) are shown for antitumor immunity ($a < b$) with parameter set 5 from Table 1. Contour plots at various times demonstrate the dependence of tumor fate on parameter values. Blue (elim) corresponds to tumor elimination and red (esc) to tumor escape. Shades of purple in between these limits correspond to tumors of intermediate size at the given time. These intermediate contour bands (especially at 100 and 150 days in (a) and at 100 days in (b) and (c) indicate that tumor fate is susceptible to intervention early on, but that this window closes rapidly with time. This suggests that immunotherapies that modulate these parameters may need to be combined with alternate treatments to prolong these intervention windows (Color figure online)

intended to increase immune recruitment based on successful predictions of tumor elimination from Fig. 3 with parameter set 5 (say to the level of $r = 1$), may not alter tumor fate at all for parameter set 9 in Fig. 5.

5 Discussion

To investigate the role of tumor-promoting inflammation, an emerging hallmark of cancer (Hanahan and Weinberg 2011), a new mathematical model for cancer-immune interactions was presented. This framework captures both pro-angiogenic, tumor-

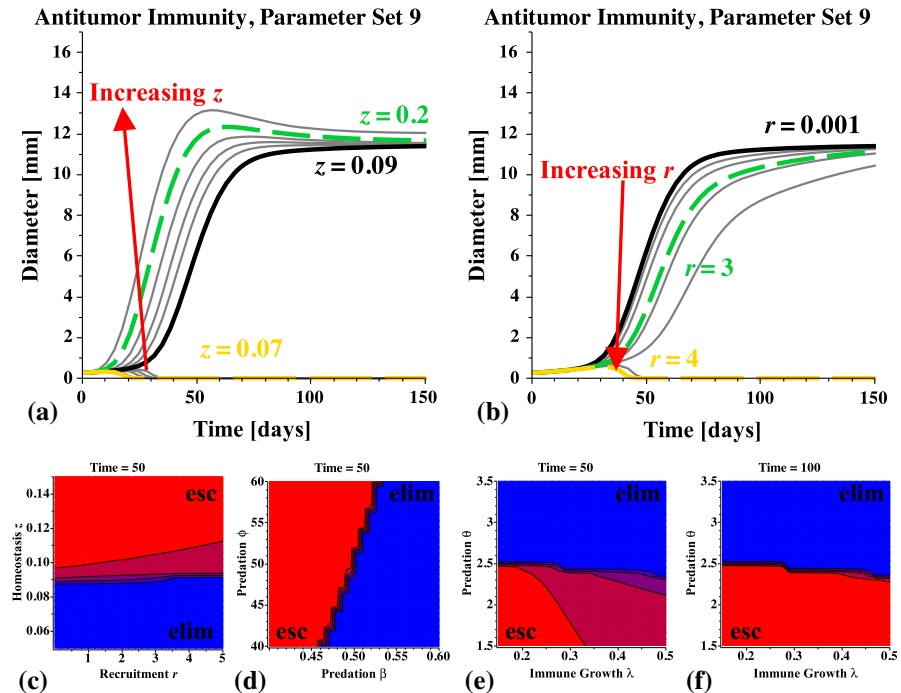


Fig. 5 Parameter sensitivity for antitumor immunity ($a < b$) and the outlier parameter set 9 from Table 1. Tumor fate is altered as the homeostasis (a) and immune recruitment (b) parameters are increased. No significant dormant periods are predicted. Contour plots of tumor fate for the parameter pairs (r, z) , (β, ϕ) , and (λ, θ) are shown in (c–e) at 50 days, as well as (λ, θ) at 100 days in (f) (Color figure online)

progressing actions and anti-angiogenic, tumor-inhibiting actions of immunity. The use of generalized logistic growth captures some of the inherent variability underlying tumor growth dynamics in an immune competent host, often neglected in macroscopic measurements and mathematical models. Model simulations suggest that two types of inflammatory responses (pro-tumor or antitumor) resolve into two fundamentally different classes of outcomes, where inflammation-enhanced tumor progression results in either a decreased tumor burden, as in the antitumor case, or an increased tumor burden, as in the pro-tumor case. Thus, near- and long-term responses of a tumor to immune interaction may be opposed; that is, a response dynamic that appears to promote growth in the near term may be superior at curtailing growth in the long-term, even to the point of establishing dormancy, while the other allows for tumor escape. Indeed, such seemingly contradictory dynamics (tumor burden decrease only following an initial increase) have been reported following immunotherapy (Wolchok et al. 2009). And a lack in understanding of the cause of such non-intuitive cancer-immune dynamics contributed to the early failures of immunotherapy trials (Hoos 2012). Our results help improve the basic understanding of cancer-immune dynamics and suggest that, in some cases, stimulated tumor growth early on may be advantageous, if it leads to a significantly smaller tumor burden. In such cases, treatments may be targeted to enhance the stability of an antitumor inflammatory environment instead of immediate tumor regression.

A Markov chain Monte Carlo method was used to estimate parameter sets that predict tumor growth equally well, but that, at the same time, also predict fundamentally different underlying dynamics. The results underscore the ultimately polar nature of final tumor fate (escape or elimination) and, at the same time, indicate that persistent regions of near-dormancy may precede either of these two outcomes. The striking variability observed across the parameter sets (see Table 1 and “Appendix 2”) demonstrates the significance of intrinsic and immeasurable factors determining the complex biological processes involved in tumor growth in an immune competent host. The underlying variability in tumor dynamics, often neglected by mathematical formulations, is captured here by generalized logistic growth with a dynamic carrying capacity. The choices made in this work for the mathematical forms in Eqs. (1)–(4), and in particular, the values of parameters a and b , determine the model dynamics and resulting biological implications discussed herein.

We propose that this variability, which is not measurable through macroscopic observations, may be due to the sensitivity of cancer cells and host stromal cells to growth and regulatory signals present in the microenvironment. Biological contributors to this variability may include the response rate of the host to pro- or anti-angiogenic signals or the strength of (or sensitivity to) the size-limiting signals originating from the tumor microenvironment (carrying capacity). Consequently, if treatment strategies are designed based on an average behavior parameter set (or patient), the treatment cannot be expected to result in the same outcome for all parameter sets (or patients). In fact, this variability may explain why treatments, including immunotherapies, work for some cases, but not all, and it emphasizes the importance of patient-specific treatment planning.

This quantitative framework also demonstrates an important and often oversimplified feature of tumor dormancy—that dormancy is a transient state. Many mathematical models predict dormancy as a stable equilibrium solution that is attained and maintained for infinite time (Wilkie 2013). The model presented here, however, describes dormancy as a transient phase that exists between tumor elimination and tumor escape, and it suggests that while treatments may prolong this state, by the fundamental nature of dormancy, the period must eventually transition to either elimination or escape. A deeper discussion on the dynamics of tumor dormancy can be found in Wilkie and Hahnfeldt (2013).

Immunotherapies, which aim to boost patient immune responses to control or eliminate the disease, have met with some success, but have failed to produce a broadly effective treatment option (Phillips 2012). The immune-stimulating drug Levamisole, for example, has been reported to inhibit tumor growth at low doses but to have no inhibitory effect, compared to control, at high doses (Sampson et al. 1977). This dose–response may result from small doses enhancing the antitumor immune response, while large doses over stimulate the response, promoting a conversion from antitumor to pro-tumor immunity, and ultimately enhancing tumor development. Such hypotheses highlight the need for theoretical investigation of treatment targets, dose–response, and dose–scheduling in treatment planning, which can be performed with our proposed framework since both direct tumor-inhibiting and direct tumor-promoting mechanisms of the immune response are considered. The model simulations and results discussed here suggest that key factors for improved tumor control by immunotherapies include

an understanding (and incorporation) of patient-specific inherent variability in tumor growth dynamics, consideration of the type of immune response active within the tumor microenvironment (pro-tumor versus antitumor), and optimal treatment targets, dosages, and schedules (the subject of ongoing work).

Acknowledgements The authors would like to thank Dr. M. La Croix for his helpful discussions and for creating Fig. 1. The work of K.W. and P.H. was supported by the National Cancer Institute under Award Number U54CA149233 (to L. Hlatky) and by the Office of Science (BER), U.S. Department of Energy, under Award Number DE-SC0001434 (to P.H.). The content is solely the responsibility of the authors and does not necessarily represent the official views of the National Cancer Institute or the National Institutes of Health.

Appendix 1

See Fig. 6.

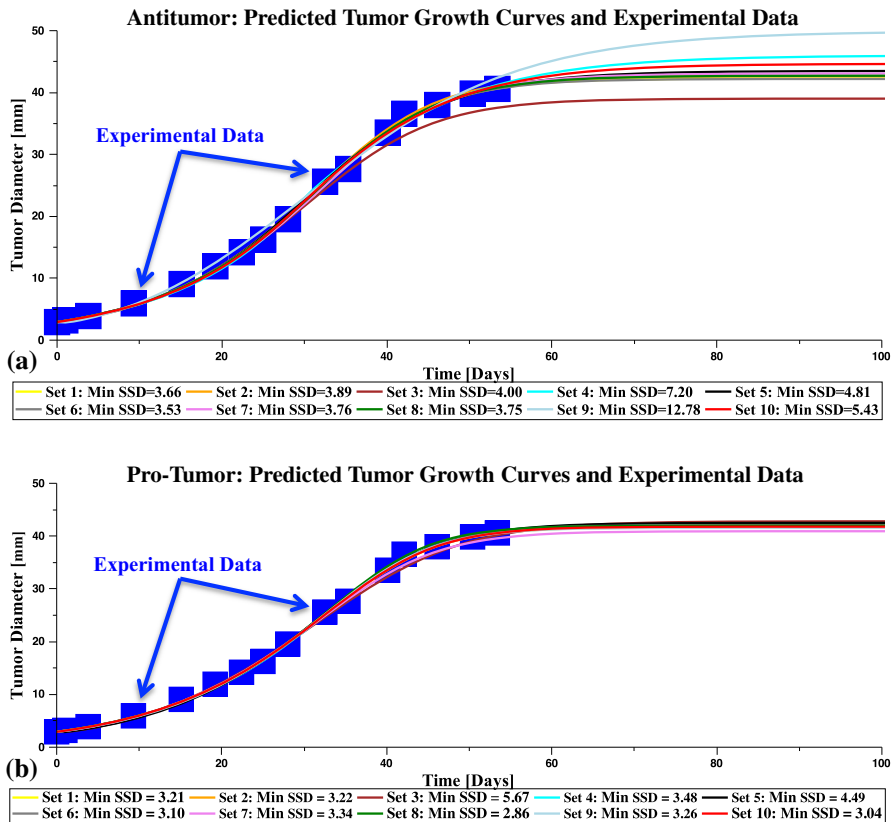


Fig. 6 Results of the data fitting: predicted tumor growth curves are shown over-laid with the experimental data for both antitumor and pro-tumor parameter set ensembles. Values of the parameters for each set are listed in Table 1 (Color figure online)

Appendix 2

See Fig. 7.

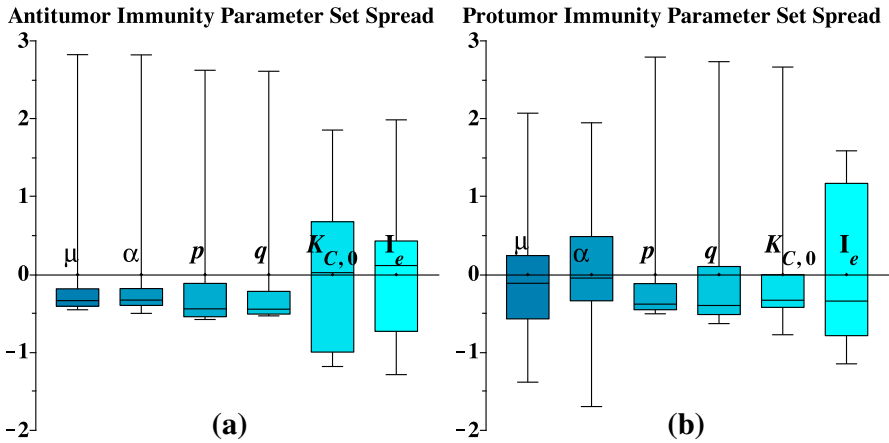


Fig. 7 Box plots showing the variability in the pro-tumor and antitumor parameter ensembles. Parameter values are rescaled for easier comparison by the normalization formula: $x_i \rightarrow \frac{x_i - \mu_x}{\sigma_x}$ where μ_x is the average, and σ_x is the standard deviation, of the set of values for parameter x (Color figure online)

Appendix 3

See Fig. 8.

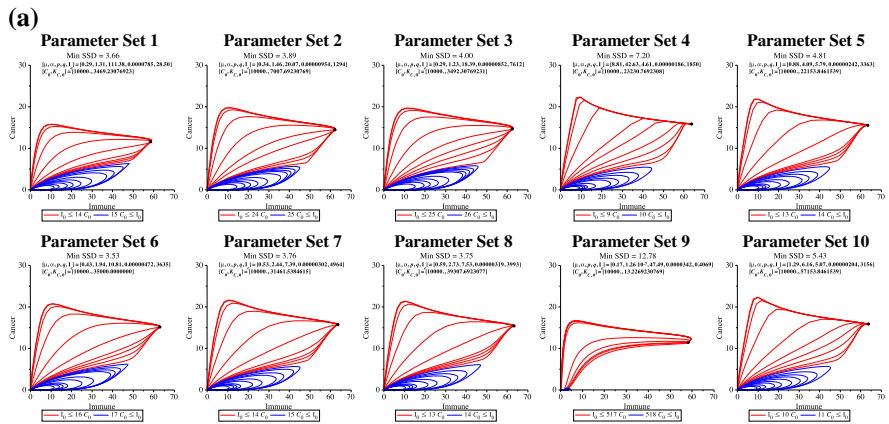


Fig. 8 Cancer-immune phase portraits demonstrate the variability across the 10 parameter sets in the antitumor (a) and pro-tumor (b) immunity ensembles (values listed in Table 1). Tumors are simulated to grow from an initial injection of $C_0 = 10^4$ cancer cells and varying numbers of immune cells ($I_0 = \gamma C_0$). The ranges (values of γ) that divide the behavior between tumor growth (red) or tumor suppression (blue) are listed below the plots. Simulations result from solving the full system of equations (1)–(4) with direct predation through Ψ , Eq. (5). Axes indicate diameter of spherical population in mm (Color figure online)

- Eftimie R, Bramson JL, Earn DJ (2010) Interactions between the immune system and cancer: a brief review of non-spatial mathematical models. *Bull Math Biol* 73(1):2–32
- Enderling H, Hlatky LR, Hahnfeldt P (2012) Immunoeediting: evidence of the multifaceted role of the immune system in self-metastatic tumor growth. *Theor Biol Med Model* 9:31
- Grivennikov SI, Greten FR, Karin M (2010) Immunity, inflammation, and cancer. *Cell* 140(6):883–899
- Hahnfeldt P et al (1999) Tumor development under angiogenic signaling: a dynamical theory of tumor growth, treatment response, and postvascular dormancy. *Cancer Res* 59:4770–4775
- Hanahan D, Weinberg RA (2011) Hallmarks of cancer: the next generation. *Cell* 144(5):646–674
- Hoos A (2012) Evolution of end points for cancer immunotherapy trials. *Ann Oncol* 23(Suppl 8):viii47–viii52
- Jackaman C et al (2003) IL-2 intratumoral immunotherapy enhances CD8+ T cells that mediate destruction of tumor cells and tumor-associated vasculature: a novel mechanism for IL-2. *J Immunol* 171(10):5051–5063
- Ji R-C (2012) Macrophages are important mediators of either tumor- or inflammation-induced lymphangiogenesis. *Cell Mol Life Sci* 69(6):897–914
- Joshi B et al (2009) On immunotherapies and cancer vaccination protocols: a mathematical modelling approach. *J Theor Biol* 259(4):820–827
- Kareva I, Wilkie KP, Hahnfeldt P (2014) The power of the tumor microenvironment: a systemic approach for a systemic disease. In: *Mathematical oncology 2013. Modeling and simulation in science, engineering and technology*. Springer, New York, pp 181–196
- Kirschner DE, Panetta JC (1998) Modeling immunotherapy of the tumor-immune interaction. *J Math Biol* 37(3):235–252
- Koebel CM et al (2007) Adaptive immunity maintains occult cancer in an equilibrium state. *Nature* 450(7171):903–907
- Kraus S, Arber N (2009) Inflammation and colorectal cancer. *Curr Opin Pharmacol* 9(4):405–410
- Kuznetsov VA (1988) Mathematical modeling of the development of dormant tumors and immune stimulation of their growth. *Cybern Syst Anal* 23(4):556–564
- Kuznetsov VA et al (1994) Nonlinear dynamics of immunogenic tumors: parameter estimation and global bifurcation analysis. *Bull Math Biol* 56(2):295–321
- Lefever R, Horsthemke W (1978) Bistability in fluctuating environments. Implications in tumor immunology. *Bull Math Biol* 41:469–490
- Li LM, Nicolson GL, Fidler IJ (1991) Direct in vitro lysis of metastatic tumor cells by cytokine-activated murine vascular endothelial cells. *Cancer Res* 51(1):245–254
- Louzoun Y et al (2014) A mathematical model for pancreatic cancer growth and treatments. *J Theor Biol* 351:74–82
- Mantovani A et al (2008) Tumour immunity: effector response to tumour and role of the microenvironment. *Lancet* 371(9614):771–783
- Matzavinos A, Chaplain MAJ, Kuznetsov VA (2004) Mathematical modelling of the spatio-temporal response of cytotoxic T-lymphocytes to a solid tumour. *Math Med Biol* 21(1):1–34
- Meshkat N, Anderson C, Distefano JJ (2011) Finding identifiable parameter combinations in nonlinear ODE models and the rational reparameterization of their input–output equations. *Math Biosci* 233(1):19–31
- Miao H et al (2011) On identifiability of nonlinear ode models and applications in viral dynamics. *SIAM Rev* 53(1):3–39
- Nelson D, Ganss R (2006) Tumor growth or regression: powered by inflammation. *J Leukoc Biol* 80(4):685–690
- Pardoll DM (2012) The blockade of immune checkpoints in cancer immunotherapy. *Nat Rev Cancer* 12:252–264. doi:10.1038/nrc3239
- Phillips C (2012) Clinical Trials Network aims to strengthen cancer immunotherapy pipeline. *NCI Cancer Bulletin—National Cancer Institute*. 9(4). <http://www.cancer.gov/ncicancerbulletin/022112/page6?cid=FBen+sf3319032>. Accessed 28 Feb 2012
- Prehn RT (1972) The immune reaction as a stimulator of tumor growth. *Science* 176:170–171
- Prehn RT (2007) Immunostimulation and immunoinhibition of premalignant lesions. *Theor Biol Med Model* 4(1):6
- Quesnel B (2008) Tumor dormancy and immunoescape. *APMIS* 116:685–694
- Rakoff-Nahoum S (2006) Why cancer and inflammation? *Yale J Biol Med* 79(3–4):123–130
- Raue A et al (2011) Addressing parameter identifiability by model-based experimentation. *IET Syst Biol* 5(2):120–130

- Robert CP, Casella G (2010) *Introducing Monte Carlo methods with R*. Springer, New York
- Roose T, Chapman SJ, Maini PK (2007) Mathematical models of avascular tumor growth. *SIAM Rev* 49(2):179–208
- Sampson D et al (1977) Dose dependence of immunopotential of tumor regression induced by levamisole. *Cancer Res* 37(10):3526–3529
- Takayanagi T, Kawamura H, Ohuchi A (2006) Cellular automaton model of a tumor tissue consisting of tumor cells, cytotoxic T lymphocytes (CTLs), and cytokine produced by CTLs. *IPSIJ Digit Cour* 2:138–144
- Tanooka H, Tanaka K, Arimoto H (1982) Dose response and growth rates of subcutaneous tumors induced with 3-methylcholanthrene in mice and timing of tumor origin. *Cancer Res* 42(11):4740–4743
- Wilkie KP (2013) A review of mathematical models of cancer–immune interactions in the context of tumor dormancy. In: Enderling H, Almog N, Hlatky L (eds) *Systems biology of tumor dormancy*. Springer, New York, pp 201–234
- Wilkie KP, Hahnfeldt P (2013) Tumor–immune dynamics regulated in the microenvironment inform the transient nature of immune-induced tumor dormancy. *Cancer Res* 73(12):3534–3544. <http://cancerres.aacrjournals.org/content/early/2013/03/22/0008-5472.CAN-12-4590.short>
- Wolchok JD et al (2009) Guidelines for the evaluation of immune therapy activity in solid tumors: immune-related response criteria. *Clinical Cancer Res* 15(23):7412–7420